IEEE Access
Multidisciplinary | Rapid Review | Open Access Journal

Received November 25, 2020, accepted December 19, 2020, date of publication December 28, 2020,
date of current version February 1, 2021.

*Digital Object Identifier 10.1109/ACCESS.2020.3047828*

# Continuous Estimation of Human Upper Limb Joint Angles by Using PSO-LSTM Model

**GANG TANG[1], JINQIN SHENG[1], DONGMEI WANG[2], AND SHAOYANG MEN[3]**
[1]Logistics Engineering College, Shanghai Maritime University, Shanghai 201306, China
[2]School of Mechanical Engineering, Shanghai Jiao Tong University, Shanghai 200240, China
[3]School of Medical Information Engineering, Guangzhou University of Chinese Medicine, Guangzhou 510006, China

Corresponding author: Shaoyang Men (shaoyang.men@gzucm.edu.cn)

This work was supported in part by the Medical Science and Technology Research Foundation of Guangdong under Grant A2020334, in part by the Youth Creative Talent Project (Natural Science) of Guangdong under Grant 2019KQNCX018, and in part by the Young Talent Training Project of Guangzhou University of Chinese Medicine under Grant QNYC20190110.

**ABSTRACT** Aiming at the continuous motion control problem of the upper limb auxiliary exoskeleton. In this paper, we use particle swarm optimization (PSO) to optimize the long short-term memory network (LSTM), and use the optimized network to establish a map between surface electromyography (sEMG) signals and joint angles. The inputs of the model are sEMG feature time series, which have been dimension reduction processed, and the outputs of the model are the joint angles of the elbow and wrist. To validate the effectiveness of the PSO-LSTM model, eight healthy subjects participated in the experiment. Eight channels of sEMG from eight human upper limb muscles were recorded and two joint angles including the elbow joint and wrist joint were acquired. The proposed PSO-LSTM model and back propagation neural network (BP) model were trained and tested, by using the sEMG feature time series. These time series have been processed for continuous estimation of human upper limb movements. Our experimental results showed that the proposed PSO-LSTM model could achieve a significantly lower estimation root mean square error (RMSE) than the BP model. The RMSE of PSO-LSTM is 0.0599 and the RMSE of BP is 0.1986 in the experiment of continuous elbow movement. The RMSE of PSO-LSTM is 0.1025 and the RMSE of BP is 0.2348 in the experiment of continuous wrist movement. These results suggest that the proposed PSO-LSTM model has a good performance on joint angles estimation by using sEMG feature time series that have been processed for subjects. This model would be used on rehabilitation robots for active rehabilitation of spinal cord injury (SCI) patients or stroke patients.

**INDEX TERMS** Continuous estimation, long short-term memory network (LSTM), particle swarm optimization (PSO) algorithm, surface electromyography (sEMG).

## I. INTRODUCTION

Uder the trend of population aging, more and more patients are suffering from partial paralysis caused by stroke. Many people with spinal cord injury or stroke have incomplete muscle damage. The muscle strength of their healthy limb is much greater than that of the affected limb. Taking into account the symmetry of human limbs [1], healthy limb movements can be used as control signals for rehabilitation robots to assist damaged limbs [2]. The development of powered exoskeleton robots can help patients with this neurological disorder perform various activities [3], thereby helping them restore the strength and function of their limbs [4]. Leonardis *et al.* [5] proposed a myoelectric-driven exoskeleton hand for grip training of bilateral rehabilitation after stroke, retaining the residual touch-sensing ability during grasping of real objects.

Modern human-computer interaction technology is a hot spot in current theoretical and applied research. It needs to move by the instructions from humans in the beginning, developed to the condition that robots actively understand human behavior intentions [6], which derives a new type of human-computer interaction technology based on bioelectric signals [8]. As early as the 1960s, sEMG signal was used as a source of biological signals for human-computer interaction control [9]. Since the sEMG signal contains neural control signals that can estimate movement intentions [10], [11], it has been used as a feasible and effective neural interface for interpreting human movement intentions as control commands [12]. Recognize the person's movement intention, usually including discrete action modal classification and joint

The associate editor coordinating the review of this manuscript and approving it for publication was Siddhartha Bhattacharyya.

continuous motion estimation [13]. The motion classification method [14] based on sEMG can only estimate a few discrete body movements. We can control the robot by the estimation results, but the robot joints cannot move continuously and freely like human joints. Compared with action classification, continuous motion estimation of joints is more valuable for smooth control of robot motion [15]. The continuous estimation of human joint motion is the key to realize the soft and coordinated movement of auxiliary equipment such as exoskeleton robots, active orthoses, prostheses [7].

Due to the non-linear relationship of the mapping between myoelectric signals and human motion and the non-stationarity of myoelectric signals over time, the performance of sEMG control of human-computer interaction depends heavily on the accuracy and robustness of human motion estimation [16].An effective method of sEMG signal signature extraction and estimation is important to obtain the desired kinematic and kinetic information. In order to improve the accuracy of the estimation, the primary or myopic dominant muscle for a given movement can be selected by muscle synergy when selecting the input sEMG [17]. This combination creates complex mappings between the synergies and their effects on the limb [18]. Thus, extracting features from the input signal is essential to provide descriptive synergistic input to the control scheme describing these mappings.

Whereas sEMG is a weak electrical potential generated by muscle cells when they are electrically or neurologically activated [19]. Usually, the time-domain feature signals of the sEMG signal, such as mean absolute value (MAV) is the average value of the amplitude's absolute value of the sEMG signal, waveform length (WL) describes the complexity of sEMG signals, and zero-crossing point (ZC) is an important feature defined in the time-domain [20], [21]. Pan *et al.* [22] established a state space model to estimate the angle of finger joints, and extracted some time-domain characteristic signals of sEMG signals (MAV, WL, and ZC) to represent the sEMG signal effect. Synergistic time-domain features are simultaneous extractions of information from multiple sEMG signal channels to characterize the principles that represent potential muscle coordination during the execution of various movements [23]. Several combinations of these time-domain features are commonly used for continuous motion estimation. However, most of the features are redundant, which does not significantly improvement estimation accuracy but rather makes the spatial dimension of the input features too high [24]. Muceli and Farina [25] applied Principle component analysis to control a 4-DOF wrist with more comprehensive and lower-dimensional synergy inputs.

Currently, many researchers use regression models to establish the mapping to enable estimation of continuous joint angles, which is between sEMG signals and joint angles. Zhang *et al.* [26] proposed an m-order non-linear model is aim to establish the mapping between the sEMG signal and the human leg joint angle, and to estimate the human leg joint angle by Back Propagation neural network (BP). Wang *et al.* [27] proposed to use the wavelet packet energy entropy of special subspaces as a feature of sEMG signals to estimate shoulder and elbow joint angles using a genetic an Elman neural network optimized by a genetic algorithm. Ma *et al.* [28] proposed a short connected autoencoder long short-term memory (SCA-LSTM) model that uses kinematic information extracted from the sEMG to estimate continuous arm motion. Chen *et al.* [29] proposed a deep belief network that consist of restricted Boltzmann machines for low-dimensional spatial encoding of sEMG signals after multichannel processing. The BP neural network maps the optimal sEMG signal features to finite element joint angles. The above methods have improved the accuracy of estimation to a certain degree. However, only the BP model describes the training time. The proposed method of this research is applied to real-time rehabilitation systems, training time is an indicator to improve real-time performance, so this paper uses the BP model for comparison. The LSTM model has a good effect on time series estimation [30]. Also, the particle swarm optimization (PSO) algorithm is a commonly used optimization algorithm, which has the advantage of implement the model easily [31]. In order to improve the estimation accuracy, using PSO algorithm to optimize LSTM model is a feasible strategy. Therefore, we want to use PSO-LSTM to establish an estimation model of the upper limb joint angle to estimate for providing an interface for active training of the contralateral upper limb.

This paper includes four sections in total and these sections are arranged as follows: Section 2 talks about the proposed method, to be more specific, it introduces the acquisition of upper limb kinematics data and sEMG data as well as the joint angles calculation, sEMG data processing, and PSO-LSTM network construction, as shown in Fig. 1, the process of sEMG based joint angle estimation. Section 3 describes the experimental results and comparison of accuracy and training time between the BP model and the PSO-LSTM model. Finally, Section 4 concludes the paper and draws a few perspectives for further work.

## II. METHODS

### A. DATA ACQUISITION

Eight healthy male subjects (age 22-27, height 172-180 cm, weight 61-75 kg) were enrolled in this study. They are right-handers. This paper studies the sEMG data and movement data of the subjects' right upper limbs as examples because the human body can be considered as symmetry to a certain extent. All the subjects read and signed an informed consent form approved by an institutional review board. In this experiment, a NDI Optotrak certus optical motion capture system (NDI, Canada) was used to track the participants' movement at a rate of 100 Hz. Positions of the markers are listed in Tab. 1. The subject performs warm-up activities, first doing systemic warm-up activities. About 5 minutes before each experiment, preheat the electromyograph (ATM-8) system for about 0.5 hours and put the system on standby. Perform initial settings for the sEMG, including clearing, etc.

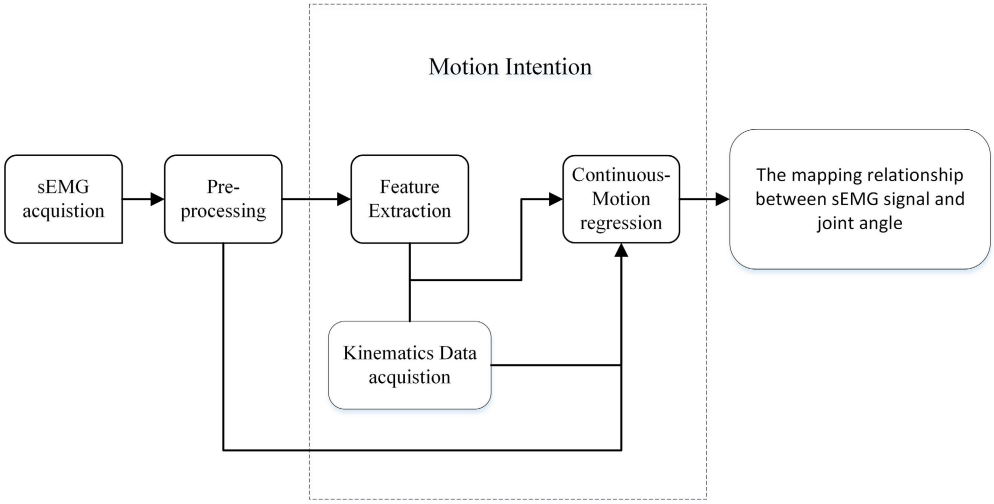


**FIGURE 1.** The process of sEMG based joint angle estimation.

**TABLE 1.** Positions of the markers.

| number | marker name | Location |
|---|---|---|
| 1 | RAC | Right acromion center |
| 2 | LAC | Left acromion center |
| 3 | EL | Most caudal point on lateral epicondyle |
| 4 | EM | Most caudal point on medial epicondyle |
| 5 | RS | Most caudal point on radial styloid |
| 6 | US | Most caudal point on ulnar styloid |
| 7 | LH | Distal head of the second metacarpal |
| 8 | MH | Distal head of the fifth metacarpal |

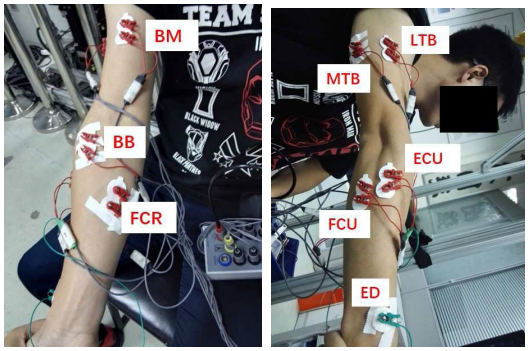


(a) front (b) back

**FIGURE 2.** sEMG electrode layout.

Determine the electrode placement point: the position of the surface electrode is the same as the direction of the muscle fiber, and it is attached to the muscle belly of the tested muscle according to the requirements of the SENIAM protocol. In order to record sEMG and joint angle movement signals associated with the targeted upper limb movements (particularly the elbow and wrist joint angles), eight sEMG wireless signal sensors were placed on the extensor digitorum (ED), extensor carpi ulnaris (ECU), flexor carpi ulnaris (FCU), flexor carpi radialis (FCR), brachioradialis muscle (BM), biceps brachii (BB), lateral head of triceps brachii (LTB), and medial head of triceps brachii (MTB) of the participants' dominant arm, respectively, as shown in Fig. 2.

Before the experiment begins, each subject should be familiar with the experimental environment and various types of movement. In the experiment, the subjects try to relax and complete the movement naturally. After processing the sEMG and movement data, all will be used to train between sEMG and movement mapping, make cross-validation of joint motion estimations.

In the experiment, the subject was first asked to sit on a chair with the upper limbs vertically relaxed in the sagittal plane, as in Fig. 3 (a) Second, there were a total of five movements, as in Fig. 3 (b) Elbow Flexion/Extension (EFE), in which the subject bent the forearm initially vertically to the point of maximum forearm flexion. After holding the forearm in the horizontal position for 2 seconds, the subject was asked to extend the forearm to the initial vertical position. As in Fig. 3 (c) Elbow Pronation/Supination (EPS), the subject will initially horizontal to forearm pronation to maximum, and then the subject will be asked to horizontal to forearm supination to maximum. As in Fig. 3 (d) Wrist Flexion/Extension(WFE), The subject relaxed the upper limb vertically and flexed and extended the wrist as far as it felt comfortable to do so. As in Fig. 3 (e) Wrist Adduction/Abduction (WAA), The subject again relaxes the upper extremity vertically, with maximum adduction and abduction wrist as felt comfortable. As in Fig. 3 (f) Continuous motion of the Elbow and Wrist (CEW), the subject relaxes the upper limb vertically and, as far as feels comfortable, first internally rotates the elbow and wrist joints simultaneously to their maximum extent, then flexes the forearm to its maximum extent before extending the forearm to its maximum extent.

### B. DATA PROCESSING

#### 1) MOTION DATA PROCESSING

In this paper, we take the elbow and the wrist of the upper limb as an example to exhibit the method procedure.

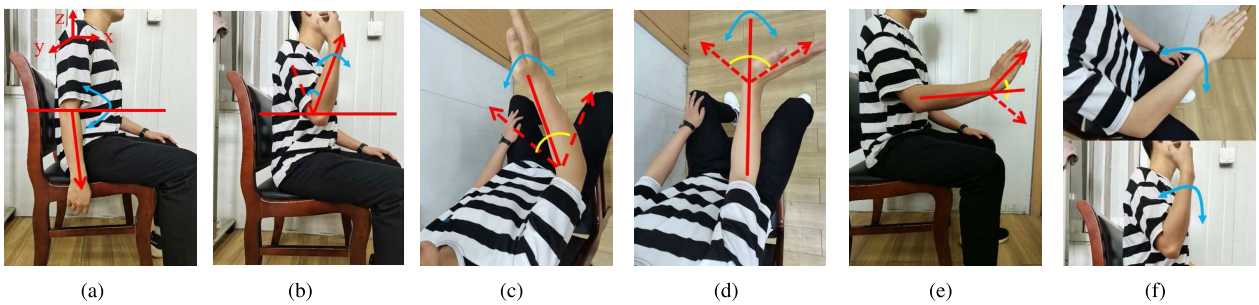


**FIGURE 3.** joint position (a)Keep it free-standing, (b)Elbow flexion/extension, (c)Elbow pronation/supination, (d) Wrist flexion/extension, (e)Wrist adduction/abduction, (f)Continuous motion of the elbow and wrist.

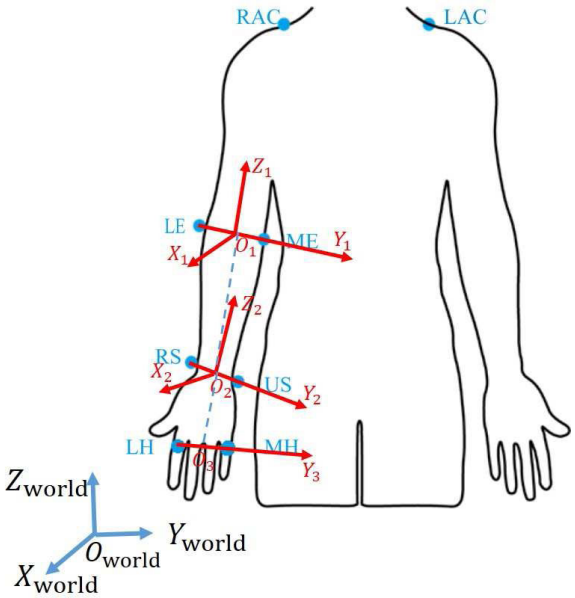


**FIGURE 4.** Coordinate conversion of human right upper limb motion marker points and joint angle calculation.

The calculation of joint angles is based on the motion trajectory, which is collected by the optical motion capture system. Including the establishment of the coordinate system, the establishment of the kinematic model and the calculation of the joint angles. The first step is the definition of the coordinate system, the world coordinate system used for motion data acquisition, and the coordinate system is usually fixed. Each body segment is pasted with two non-linear reflection marker points (assuming the body segment is rigid), and the corresponding physiological coordinate system of the skeleton is established on the basis of the reflection marker points. The physiological coordinate system is established by the reflection marker points located at the bony-centric prominence of each body segment and the relevant anthropometric parameters, and the x, y and z axes are generally set in the sagittal, cross-sectional and coronal planes. As shown in Fig. 4, as an example to calculate the angle of the right upper limb wrist joint in a single person, a physiological coordinate system was established using reflective marker points, with the midpoints of the two reflective marker points LE and ME at the central prominence of the elbow bone as $O_1$, and the midpoint of the two reflection marker points RS, US at the bony-centric prominence of the wrist joint is $O_2$, connecting $O_1$, $O_2$, with $\overrightarrow{O_2O_1}$ as the positive direction of $\overrightarrow{Z_1}$, and $\overrightarrow{LE}, \overrightarrow{ME}$ as the positive direction of $\overrightarrow{Y_1}$, then the $\overrightarrow{X_1}$ is a vector perpendicular to $\overrightarrow{Y_1}$ and $\overrightarrow{Z_1}$. Similarly, a physiological coordinate system was established at the wrist joint. $O_3$ at the midpoint where the second distal metacarpal head reflective marker point LH and the fifth distal metacarpal reflective marker point MH of the hand are connected. connecting $O_3$, $O_2$, with $\overrightarrow{O_3O_2}$ as the positive direction of $\overrightarrow{Z_2}$.

Since the focus of this study is on the estimation of joint motion in the sagittal plane, the calculation of the wrist joint angle requires the conversion of the reflective marker points collected in the world coordinate system to the location of the physiological coordinate system. Therefore, the calculated joint angle corresponds to the motion of the upper extremity elbow and wrist joints in the sagittal plane.

To simplify the calculation, the two rigid bodies are assumed to be two line segments. These are $l_{O_2O_1}$ and $l_{O_2O_3}$. The reflective marker points on the world coordinate system obtained by optical motion capture are converted to the physiological coordinate system $X_2\ Y_2\ Z_2$, and then $\overrightarrow{l''_{O_2O_1}}$ is projected onto the $X_2\ O_2\ Z_2$ plane (sagittal plane) to obtain $\overrightarrow{l''_{O_2O_1}}$. Then the angle between $\overrightarrow{l''_{O_2O_1}}$ and $\overrightarrow{l_{O_2O_3}}$ on $X_2\ O_2\ Z_2$ is the carpal joint angle $\theta_{WFE}$.

### 2) sEMG DATA PROCESSING

In the data acquisition experiment, we set the sampling frequency of the sEMG signal to 1000 Hz. The acquisition frequency of the real-time angle signal is 100 Hz. In order to unify the signal frequency, we adopt the average sub-sampling processing method. In order to improve the signal-to-noise ratio of the signal, the collected sEMG signal must be preprocessed. First, perform 50Hz notch processing on the original sEMG signal, in order to remove power frequency interference. Second, use a high-pass filter to remove low-frequency interference caused by cable movement and muscle movement. Then full-wave rectification to make the signal amplitude greater than 0. After that, use a low-pass filter to remove high-frequency signals, so that the frequency distribution of sEMG signal is similar to the frequency distribution of joint angle. Finally, the signals from each muscle were normalized with respect to their maximum

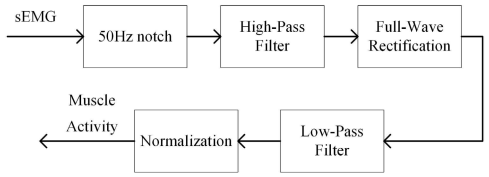


**FIGURE 5.** The process of extracting muscle activation.

voluntary isometric contraction value (MVC). Fig. 5 shows the entire process, with which we have extracted the muscle activity (MA) from raw sEMG signals.

Using the normalized sEMG signal to solve for the neural activation strength $u(t)$, the equation is as follows:

$$u(t) = \alpha \cdot e(t-d) - \beta_1 \cdot u(t-1) - \beta_2 \cdot u(t-2) \quad (1)$$

where e(t) is the sEMG value after preprocessed; u(t) is neural activation; d is the electromechanical delay, and let d=10ms; $\alpha$, $\beta_1$, and $\beta_2$ are coefficients that define the second-order dynamics. To realize a positive stable solution, a set of constraints has to be employed. $\gamma_1 = 0.5$ and $\gamma_2 = 0.5$ in this article.

$$\begin{cases} \beta_1 = \gamma_1 + \gamma_2; \\ \beta_2 = \gamma_1 \cdot \gamma_2; \\ \alpha - \beta_1 - \beta_2 = 1; \\ |\gamma_1| < 1; \\ |\gamma_2| < 1. \end{cases} \quad (2)$$

There exists the non-linear relationship between neural activation u(t) and muscle activation, especially in the condition of low level sEMG. We proposed a simple transformation as Eq.3 to indicate this non-linear relationship. A is the non-linear shape factor allowed to vary between $-3$ and 0. A=-1.5 in this article.

$$a(t) = \frac{e^{Au(t)} - 1}{e^{A} - 1} \quad (3)$$

Time-domain, frequency-domain features have been used for the analysis and processing of sEMG signals. Therefore, we selected five commonly used time-domain and two commonly frequency-domain features to establish feature vectors. These time-domain features were the mean absolute value (MAV), root mean square (RMS), variance (VAR), zero crossings (ZC), and waveform length (WL). These frequency-domain features were the mean power frequency (MPF) and median frequency (MF). The seven sEMG features are described below:

1) MAV

$$MAV(i) = \frac{1}{N} \sum_{i=1}^{N} |emg_i| \quad (4)$$

2) RMS

$$RMS(i) = \sqrt{\sum_{i=1}^{N} emg_i^2} \quad (5)$$

3) VAR

$$VAR(i) = \frac{1}{N-1} \sum_{i=1}^{N} (emg_i - emg_m)^2 \quad (6)$$

4) ZC

$$ZC(i) = \sum sgn(-emg_i * emg_(i+1)) \quad (7)$$

$$sgn(emg) = \begin{cases} 1, & \text{if } emg>0 \\ 0, & \text{if others} \end{cases} \quad (8)$$

5) WL

$$WL(i) = \frac{1}{N} \sum_{i=1}^{N-1} |emg_{i+1} - emg_i| \quad (9)$$

where, $emg_i (i = 1, 2, \ldots, N)$ is the time series of sEMG signals of length N. $emg_m$ is the integrated electromyography value of the sEMG signals.

6) MPF

$$MPF = \frac{\int_0^{\infty} fP(f)\, df}{\int_0^{\infty} P(f)\, df} \quad (10)$$

7) MF

$$\int_0^{MF} P(f)\, df = \frac{1}{2} \int_0^{\infty} P(f)\, df \quad (11)$$

where, $P(f)$ is the power spectral density function of the signal.

### C. sEMG SIGNAL CORRELATION ANALYSIS

Each joint movement corresponds to a different synergistic muscle, and there is a clear distinction between these synergistic muscles due to the different modes of movement to which they belong. Therefore, the synergistic muscles associated with the movement can be obtained by calculating the linear correlation between the activation of the muscles and the movement. The linear correlation coefficient is calculated as follows:

$$r(MA(t), T(t)) = \frac{Cov(MA(t), T(t))}{\sqrt{Var[MA(t)]\, Var[T(t)]}} \quad (12)$$

where, $r$ is the linear correlation coefficient between muscle activation and joint angle, $MA(t)$ is muscle activation, $T(t)$ is target joint angle, $Var[MA(t)]$ is the variance of muscle activation as a function of angle, $Var[T(t)]$ is the variance of the target joint angle as a function of angle, $Cov(MA(t), T(t))$ is the covariance between muscle activation and joint angle.

High dimensional features were prone to multicollinearity problems and reduced estimation model performance. It could also lead to a long time requirement of model training and reduced real-time performance of online estimation. Correlation analysis of features could find completely related features and delete them to eliminate possible multicollinearity issues. Since the features we extracted did not fit the normal distribution, we chose the Spearman correlation coefficient for correlation analysis, which is calculated as:

$$\rho = 1 - \frac{6 \sum d_i^2}{n(n^2 - 1)} \quad (13)$$

where, $n$ is the number of samples, $d_i$ is the rank difference after the ranked original data.

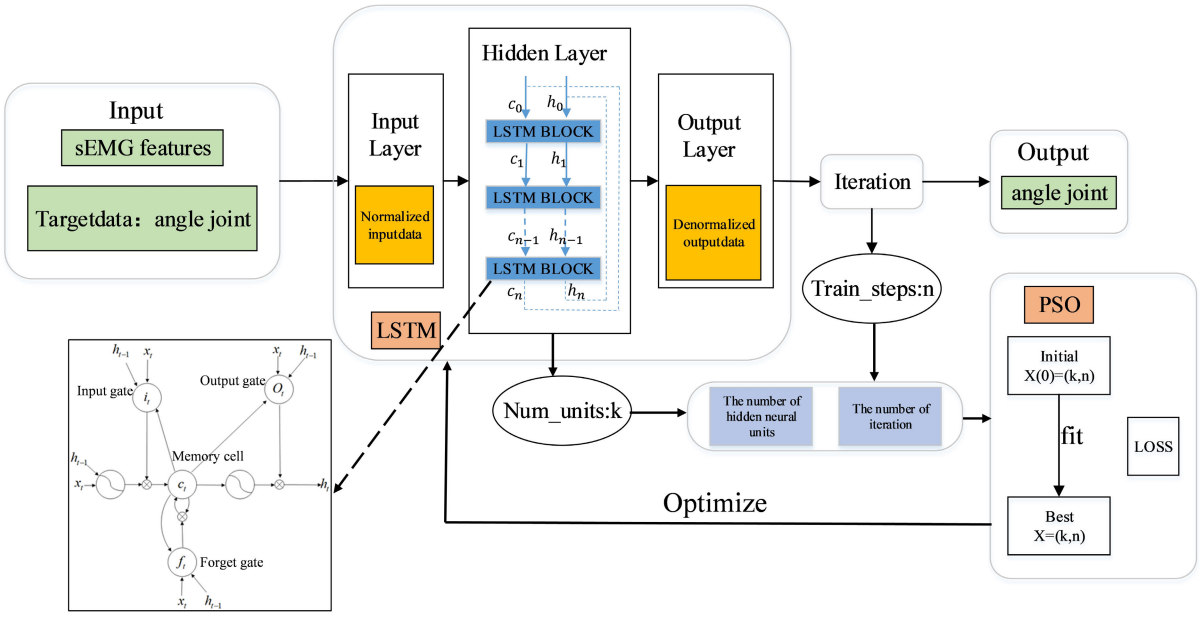


**FIGURE 6.** PSO-LSTM Joint angle estimation algorithm flow.

### D. PSO-LSTM FOR JOINT ANGLE ESTIMATION

In this study, the LSTM network estimation model was constructed with two parameters, the number of hidden neurons (Num_ units) and the number of iterations (Train_ steps) in the LSTM model, which were optimized using the PSO algorithm. The model was finally applied to the upper limb joint angle estimation. The modeling and optimization process is shown in Fig. 6.

#### 1) JOINT ANGLE ESTIMATION BASED ON LSTM

LSTM is essentially an improvement on the basic Recurrent neural network (RNN) structure, but the structure of the Memory Cell module in the implicit part is different from RNN. Three important gate control functions are reintroduced in the Memory Cell module, namely, forgetting gate, input gate, and output gate. Oblivion gate $f_t$ determines how much information should be discarded from the previous memory cell, update gate $i_t$ determines how much information should be stored in the new memory cell, and output gate $o_t$ is responsible for updating the current implicit state.

The forget gate excitation function is usually a logarithmic logistic curve, so the oblivion gate excitation is evaluated [0,1], if $f_t = 0$ means that all unit's states are forgotten for the previous moment, otherwise if $f_t = 1$ means that all unit's states are forgotten for the previous moment. Usually,v the value of $f_t$ is (0,1), and only the unit's states of the previous moment are remembered. Information to be saved. The main model formula for LSTM is as follows.

$$f_t = \sigma\left(W_f \cdot [h_{t-1} \cdot x_t] + b_f\right) \tag{14}$$

$$i_t = \sigma\left(W_i \cdot [h_{t-1} \cdot x_t] + b_i\right) \tag{15}$$

$$\tilde{c_t} = \tanh\left(W_c \cdot [h_{t-1} \cdot x_t] + b_c\right) \tag{16}$$

$$c_t = f_t * c_{t-1} + i_t * \tilde{c}_t \tag{17}$$

$$o_t = \sigma\left(W_o \cdot [h_{t-1} \cdot x_t] + b_o\right) \tag{18}$$

$$h_t = o_t * \tan h\left(c_t\right) \tag{19}$$

where $h_{t-1}$ is the unit's state at the previous moment, $x_t$ is the input at the current moment, $f_t$ is the output expression of the forget gate at timet; $i_t$ is the output expression of the input gate at timet; $o_t$ is the output expression of the output gate at timet; $\tilde{c_t}$ is the state value of the memory Cell at time t. $h_t$ is the output expression of memory cell at time t. $W_f$, $W_i$, $W_c$, $W_o$ is weight matrix, $b_f$, $b_i$, $b_c$, $b_o$ is the bias. $\sigma$ is the sigmoid activation function of the forget gate. tanh is the forget gate activation function.

Since the joint angle is related to the sEMG signal, to ensure the accuracy of the LSTM model estimation, we used the target joint angle and the features of the sEMG signal as the input to the model to predict the joint angle. The input vector expressions are as follows.

$$x(t) = [T(t), F_{sEMG}(t)] \tag{20}$$

where, $x(t)$ is the input of the LSTM Model, $T(t)$ is the target joint angle, $F_{sEMG}(t)$ is a processed sEMG signal features.

The estimation model of the LSTM network based on a deep neural network contains a hidden network. The number of neurons in the hidden network is difficult to determine, and the number of iterations will directly affect the estimation effect. The insufficient number of iterations will lead to underfitting, and too many iterations will lead to overfitting. However, these parameters are generally set manually through experience with the number of iterations, which leads to more randomness in the estimation results. The PSO algorithm can find its own optimal solution and the globally optimized solution solution in the designed space. Therefore, in this paper, the PSO algorithm is used to optimize the parameters of the LSTM to improve the estimation accuracy.

#### 2) PSO OPTIMIZING ALGORITHM

The core idea of the PSO algorithm is to first initialize a set of random solutions and then find the optimal solution by iteratively. The two parameters of the model of LSTM

are used as the optimization seeking variables of the particle in 2 dimensions, and by constantly updating the velocity and position of the particle, the value of the adaptation of the objective function is calculated to achieve the global optimum and obtain a better model parameter. The velocity and position formula of the PSO algorithm is shown below.

$$V_{i,j}^{k+1} = wV_{i,j}^{k} + c_1 r\left(pbest_{i,j}^{k} - X_{i,j}^{k}\right) + c_2 r\left(gbest_{i,j}^{k} - X_{i,j}^{k}\right) \quad (21)$$

$$X_{i,j}^{k+1} = X_{i,j}^{k} + V_{i,j}^{k} \quad (22)$$

where, $w$ is the weight, $c_1$ and $c_2$ are the learning factors, $r$ is the random number between [0, 1]. $V_{i,j}^{k}$, $X_{i,j}^{k}$, $pbest_{i,j}^{k}$ and $gbest_{i,j}^{k}$ are the velocity component, position component, individual optimum, and population global optimum of the $i$-th particle in the $j$-th dimension in the $k$-th iteration, respectively.

In this paper, we use the non-linear decreasing inertial weighting method to improve the parameter seeking ability of the PSO algorithm.

$$w = w_{max} - (w_{max} - w_{min}) \tan\left(\frac{\Pi}{4}\frac{k}{k_{max}}\right) \quad (23)$$

where, $w_{max}$ and $w_{min}$ are the maximum and minimum values of the inertia weights, respectively, and k is the number of current generations; $k_{max}$ is the maximum number of iterations.

The PSO algorithm optimizes the LSTM parameters as follows.

Step1. The acquired sEMG signal data, movement data were preprocessed.

Step2. The particle population parameters are initialized. This includes determining the population size, the number of iterations, learning factors, and bounded intervals for the values of particle position and velocity.

Step3. The LSTM joint angle estimation model is established to determine the parameters of the seeking range. It generates a population particle. The number of neurons $k_1$, $k_2$, learning rate, and the number of training iterations $n$ as parameter variables of the model. Then the parameters set a searching range and divide the data into training, validation, and test samples.

Step4. The optimal LSTM network model is finally determined by iterative iteration. For an individual $x$, the adaptation value fit is defined as:

$$fit = 0.5\left(\frac{1}{p}\sum_{p=1}^{p}\frac{y_p - y_p'}{y_p} + \frac{1}{q}\sum_{q=1}^{q}\frac{y_q - y_q'}{y_q}\right) \quad (24)$$

where, $p$ and $q$ denotes the number of training and validation samples, $y_p$ and $y_p'$ denotes the true and estimated values of the training sample, $y_q$ and $y_q'$ denotes the true and estimated values of the validation sample.

Step5. The different particle adaptation values evaluate the particle's global optimal position pbest and local optimal position gbest. Then it is recorded as its historical best position and update common and local optimal particle positions.

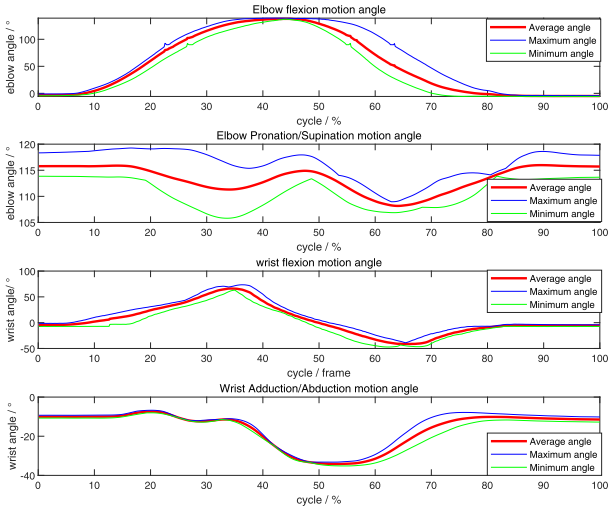


**FIGURE 7.** The results of calculation of joint angle.

Step6. If the maximum number of iterations is reached, assign the optimal parameter to train the LSTM model, and output the joint angle estimation. Otherwise, it should be returned to Step 5 and continue the execution iterations until the termination condition is met.

## III. RESULTS

All analysis results were based on data from 8 healthy subjects. Each movement does three times repetitive. One of the three repeated movements is used as the test samples, and the rest of the movements are used as the training samples. In this discussion, the angle estimation results are used to verify the model's accuracy and superiority.

### A. UPPER LIMB MOTION ANALYSIS

The test subject stands in the NDI workspace, performs the five movements on the upper limbs. It collects the position of the marker points in the world coordinate system, and then calculates the angle of each joint through the 2.2.1 subsection movement data processing method. The calculated joint angle value is used as the input $T(t)$ of the PSO-LSTM model. In order to describe the changes of joint angles corresponding to each movement, this article uses a statistical method to present these joint angle ranges. As shown in Fig. 7, this experiment is based on calculating the angle of motion of the upper limb of subject 1. The red line in the figure shows the average value of the joint angle for three repetitions. The blue and green lines show the maximum and minimum values of the joint angle for three repetitions. The calculated joint angle values were taken as the true values of the joint angles to verify the accuracy of the model.

### B. SEMG SIGNAL PREPROCESSING ANALYSIS

The sEMG signal can be noisy during the acquisition process, as shown in Fig. 8, which is the raw sEMG signals of eight muscles and two joint angles recording during a single trial for CEW movement from subject2. The preprocessed sEMG signal was used to calculate the muscle activation, as shown in Fig. 9, which results from the preprocessed sEMG signals

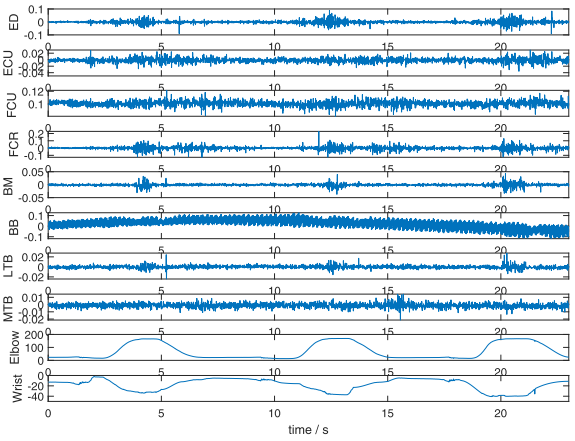


**FIGURE 8.** Raw sEMG signal recorded during a single trial for CEW movement from subject2 of the eight healthy subjects, the unit of the Y coordinate of the eight upper sub-figures is V, and the unit of the Y coordinate of the two subfigures below is a degree.

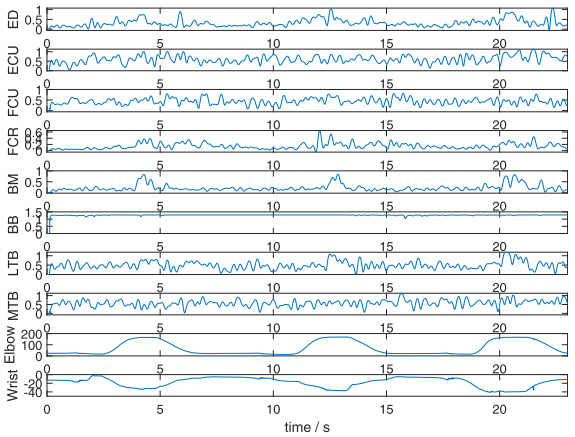


**FIGURE 9.** The results of preprocessing the sEMG data recorded during a single trial for CEW movement from subject2 of the eight healthy subjects, the unit of the Y coordinate of the eight upper sub-figures is V, and the unit of the Y coordinate of the two subfigures below is a degree.

**TABLE 2.** Correlation-based muscle activity.

| Movement abbreviation | relevant muscle |
|---|---|
| EFE | BM, BB, FCR, ECU, MTB |
| EPS | BM, FCR, ECU, MTB |
| WAA | BM, FCR, ECU |
| WFE | BM, FCR, FCU, ED, ECU, LTB |

of eight muscles and two joint angles recording during a single trial for CEW movement from subject2.

### C. CORRELATION-BASED MUSCLE ACTIVITY ANALYSIS

Since the movement of each joint corresponds to a different cooperative muscle, and the movement mode it belongs to is different, there are obvious differences between these cooperative elements. As shown in Fig. 10, the four movements are all completed under the joint action of eight muscles, and each muscle has a different degree of contribution to a specific movement mode. The muscles of each channel not only contribute to a specific movement but also contribute to multiple different movement patterns to varying degrees. As shown in Tab. 2, it means that the four movements are completed through the coordination of multichannel muscles,

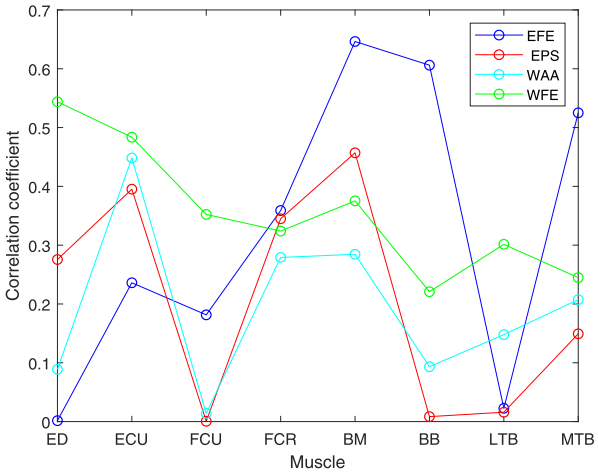


**FIGURE 10.** The results of correlations between two movements of the elbow joint and muscle activation in eight able-bodied individuals.

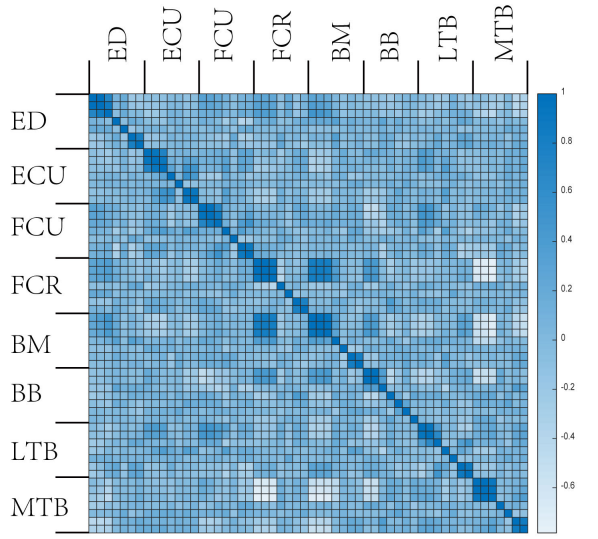


**FIGURE 11.** Correlation analysis of 56 features extracted from eight muscles. (The abscissa and ordinate represented 56 features extracted from eight different muscles. Each muscle represented its corresponding 7 features).

and different cooperative muscles are corresponding to the movement. In the subsequent analysis, the results of the analysis can be directly used to determine the synergistic muscle groups of the four movements.

The correlation analysis of eight muscle features is depicted in Fig. 11. We could easily see that highly similar features were mainly lumpy distribution and distributed on the diagonal. High correlations of features mainly occurred between different features of the same muscle, and there was almost no high correlation for features extracted from different muscles. It indicated that high correlation or multicollinearity of features was mainly related to the extracted features, and had nothing to do with the number of muscles selected and interaction between muscles. Although the multi-muscle synergy of different movements is also of great significance, we still analyze each individual movement ignored the effects of multiple-muscle synergy, and mainly analyzed the feature correlation of single muscles.

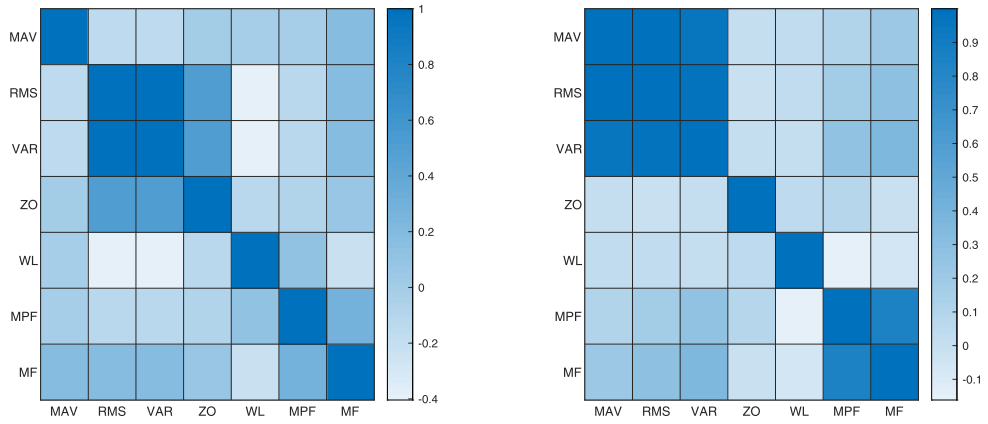


**FIGURE 12.** Correlation analysis of 7 features extracted from single muscle. (a) represented correlation analysis of features extracted from BM of subject 1, (b) represented correlation analysis of features extracted from MTB of subject 1.

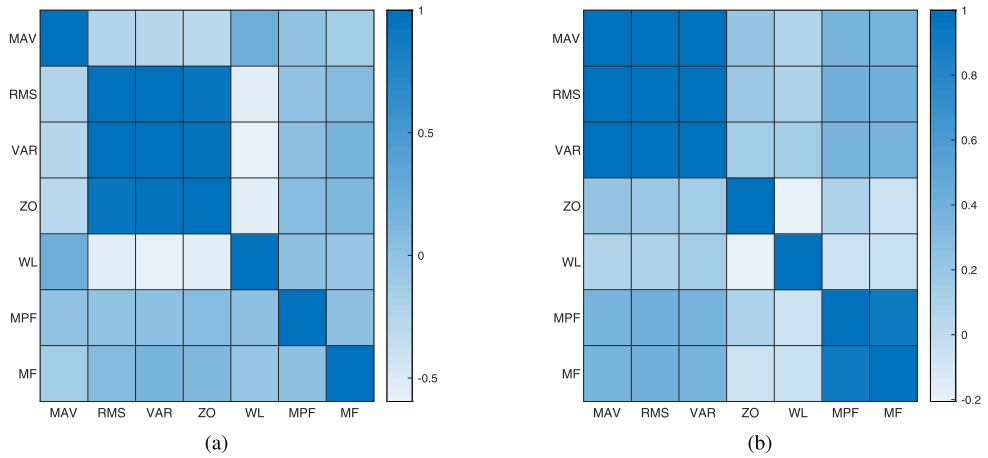


**FIGURE 13.** Correlation analysis of 7 features extracted from single muscle. (a) represented correlation analysis of features extracted from BM of subject 2, (b) represented correlation analysis of features extracted from MTB of subject 2.

Fig. 12 and Fig. 13 shows the correlation analysis between individual muscles. The correlations of the same feature between the same muscles in different subjects, and between different muscles of the same subject were not exactly the same. However, the overall feature correlation distributions were relatively similar. The correlations between RMS, VAR, ZC, WL were always high, demonstrating that these features contained very similar information. So we only kept RMS and removed the other 3 features to avoid feature redundancy and multicollinearity. Ultimately, 4 features from the original 7 features were left, and the overall feature dimension was 32 after the correlation analysis.

### D. COMPARISONS OF THE ESTIMATION RESULTS

The values of 2-dimensional target joint angle and 32-dimensional sEMG signal features are used as the input to estimate. The input vector is thirty-five, so the number of neurons in the input layer of the LSTM model is thirty-five. We use the PSO algorithm to find the optimal LSTM structural parameters. The number of particles in the PSO algorithm is set to 6, the number of iterations is 20, the learning factors $c1$ and $c2$ are 1.5, the random number $r$ is a random number in [0, 1], here it is set to 0.5, the number of neurons $k_1$ and $k_2$ are in the range of [1, 100] and [1, 100], and the number of iterations $n$ is [50-300]. With the iteration of the PSO algorithm, the number of LSTM hidden layer neurons $k_1$ is 21, $k_2$ is 14 and the number of iterations $n$ is 190.

In this paper, the average root mean square error (RMSE) and the average coefficient of determination (R2) evaluate the estimation performance. The RMSE is calculated as follows:

$$RMSE = \sqrt{\frac{\sum_{n=0}^{N} \left(y'_n - y_n\right)^2}{N}} \tag{25}$$

where $N$ is the length of the joint angle, $y'_n$ is the estimated joint angle, and $y_n$ is the real joint angle. $R^2$ is calculated as follows:

$$R^2 = 1 - \frac{\sum_{n=0}^{N} \left(y'_n - y_n\right)^2}{\sum_{n=0}^{N} \left(y_n - \overline{y_n}\right)^2} \tag{26}$$

**TABLE 3. Joint angles estimation RSME at diffenrent types of input by the eight subjects.**

| subject | Raw signal | | | | Feature signal | | | |
|---|---|---|---|---|---|---|---|---|
| | BP | | PSO-LSTM | | BP | | PSO-LSTM | |
| | Elbow | Wrist | Elbow | Wrist | Elbow | Wrist | Elbow | Wrist |
| 1 | 0.4683 | 0.5321 | 0.2511 | 0.3499 | 0.2145 | 0.2437 | 0.0701 | 0.1139 |
| 2 | 0.4311 | 0.4987 | 0.2109 | 0.3102 | 0.1901 | 0.2318 | 0.0524 | 0.1215 |
| 3 | 0.4219 | 0.4734 | 0.2099 | 0.3327 | 0.1876 | 0.2409 | 0.0489 | 0.0918 |
| 4 | 0.4624 | 0.5298 | 0.2456 | 0.3417 | 0.2078 | 0.2531 | 0.0637 | 0.1051 |
| 5 | 0.4517 | 0.5135 | 0.2311 | 0.3289 | 0.1977 | 0.2411 | 0.0627 | 0.0973 |
| 6 | 0.4216 | 0.4719 | 0.2058 | 0.3309 | 0.1823 | 0.2201 | 0.0531 | 0.1167 |
| 7 | 0.4643 | 0.5429 | 0.2498 | 0.3415 | 0.2136 | 0.2377 | 0.0678 | 0.0907 |
| 8 | 0.4418 | 0.5018 | 0.2218 | 0.3005 | 0.1956 | 0.2103 | 0.0608 | 0.0833 |
| Average | 0.4467 | 0.5080 | 0.2282 | 0.3295 | 0.1986 | 0.2348 | 0.0599 | 0.1025 |

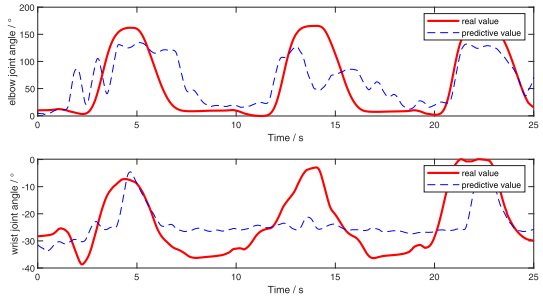


**FIGURE 14. estimation result by BP with raw input data.**

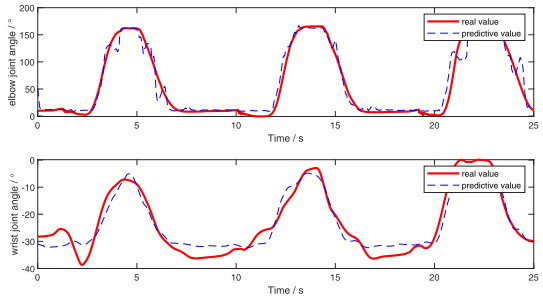


**FIGURE 15. estimation result by PSO-LSTM with raw input data.**

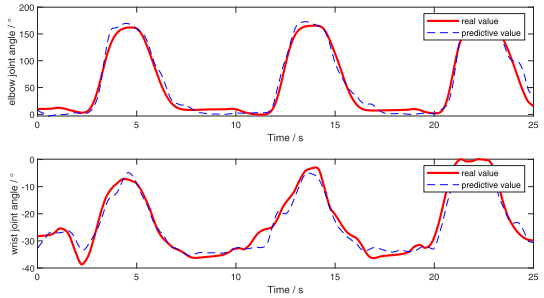


**FIGURE 16. estimation results by BP with feature extraction and dimensionality reduction input data.**

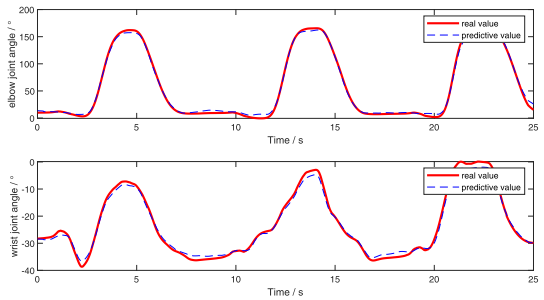


**FIGURE 17. estimation results by PSO-LSTM with feature extraction and dimensionality reduction input data.**

where $y_n$ is the real joint angle, $\overline{y_n}$ is the mean of $y_n$, and $y_n'$ is the estimated joint angle. $R^2$ is between 0 and 1. The closer this value is to 1, the better the regression fitting effect. When the fit is greater than 0.8, the model is considered to have a high fit.

In this section, the performance of the proposed PSO-LSTM model in terms of joint angle estimation was investigated and compared with that of the BP model. Simultaneously, to verify the advantages of the feature extraction method proposed in this paper, each model was validated using the raw sEMG signals and preprocessed sEMG signal as input per time. Raw sEMG signal were projected as input into the BP ( Fig. 14) and PSO-LSTM model ( Fig. 15) for testing. From the obtained results, it could be observed that the proposed PSO-LSTM model has a visibly better fitting ability than the BP model. Then, feature sEMG signals were projected as input into the BP ( Fig. 16) and PSO-LSTM model ( Fig. 17) for testing. From the results obtained, it can be seen that the proposed feature extraction method has a significantly better fit of the feature sEMG signal as input to the model than the raw sEMG signal as input to the model.

The results of the RMSE between the measured and estimated joint angles by BP and PSO-LSTM model are as shown in Tab. 3. When the raw sEMG signal is used as the input of the model, the continuous estimation RMSE of the BP($Elbow_{RMSE} = 0.4467, Wrist_{RMSE} = 0.5080$) model is significantly higher than that of the PSO-LSTM($Elbow_{RMSE} = 0.2282, Wrist_{RMSE} = 0.3295$) model. When the feature sEMG signal is used as the input of the model, the continuous estimation RMSE of the BP($Elbow_{RMSE} = 0.1986, Wrist_{RMSE} = 0.2348$) model is significantly higher than that of the PSO-LSTM($Elbow_{RMSE} = 0.0599, Wrist_{RMSE} = 0.1025$) model. The results of the $R^2$ between the measured and estimated joint angles by BP and PSO-LSTM model are then show in Tab. 4. When the raw sEMG signal is used as the input of the model, the continuous estimation $R^2$ of the BP ($Elbow_{R^2} = 0.7049, Wrist_{R^2} = 0.6998$)model is significantly lower than that of the PSO-LSTM($Elbow_{R^2} = 0.9443, Wrist_{R^2} = 0.8924$) mode. When the feature sEMG signal is used as

**TABLE 4. Joint angles estimation $R^2$ at diffenrent types of input by the eight subjects.**

| subject | Raw signal | | | | Feature signal | | | |
|---|---|---|---|---|---|---|---|---|
| | BP | | PSO-LSTM | | BP | | PSO-LSTM | |
| | Elbow | Wrist | Elbow | Wrist | Elbow | Wrist | Elbow | Wrist |
| 1 | 0.7292 | 0.6901 | 0.9338 | 0.8881 | 0.9513 | 0.9368 | 0.9901 | 0.9867 |
| 2 | 0.7551 | 0.7001 | 0.9510 | 0.8967 | 0.9656 | 0.9390 | 0.9971 | 0.9812 |
| 3 | 0.7633 | 0.7119 | 0.9543 | 0.8901 | 0.9678 | 0.9371 | 0.9978 | 0.9891 |
| 4 | 0.7135 | 0.6973 | 0.9378 | 0.8893 | 0.9561 | 0.9301 | 0.9924 | 0.9873 |
| 5 | 0.7347 | 0.6981 | 0.9392 | 0.8934 | 0.9609 | 0.9373 | 0.9931 | 0.9881 |
| 6 | 0.7671 | 0.7133 | 0.9576 | 0.8905 | 0.9691 | 0.9441 | 0.9969 | 0.9853 |
| 7 | 0.7216 | 0.6882 | 0.9376 | 0.8897 | 0.9521 | 0.9389 | 0.9908 | 0.9892 |
| 8 | 0.7431 | 0.6997 | 0.9432 | 0.9015 | 0.9612 | 0.9509 | 0.9963 | 0.9903 |
| Average | 0.7409 | 0.6998 | 0.9443 | 0.8924 | 0.9605 | 0.9392 | 0.9943 | 0.9871 |

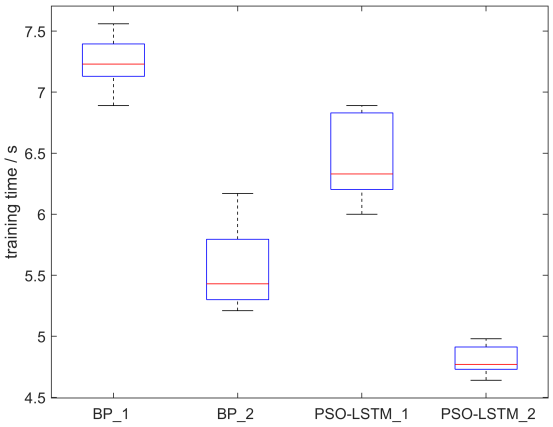


**FIGURE 18. Comparison of training time of different models and different inputs. BP_1 represents the training time of raw data as BP input, BP_2 represents the training time of feature data as BP input, PSO-LSTM_1 represents the training time of raw data as PSO-LSTM input, PSO-LSTM_2 represents the training time of feature data as PSO-LSTM input.**

the input of the model, the continuous estimation $R^2$ of the BP($Elbow_{R^2} = 0.9605, Wrist_{R^2} = 0.9392$) model is significantly lower than that of the PSO-LSTM($Elbow_{R^2} = 0.9943, Wrist_{R^2} = 0.9871$) model. The research shows that the proposed PSO-LSTM model with feature sEMG signals as inputs allows for an adequate estimation of the joint angular motion. At the same time, it can be seen that in the process of continuous joint angle estimation, the estimation error of the elbow joint angle is significantly lower than that of the wrist joint. This result shows that when the wrist and elbow joints move continuously, the estimation accuracy will be affected. After feature extraction and dimensionality reduction, the data is used as input. It can be clearly seen that the training time is reduced, as shown in Fig. 18. Moreover, the training time of the PSO-LSTM model is shorter than the BP model. Reducing the training time can improve the response speed of the system, thereby improving the real-time characteristics.

The results present that the joint angles of the human upper limb can be well estimated by the sEMG signals when people make the continuous motion of the Elbow and Wrist movement. The joint angles estimation by using feature sEMG signal as input for PSO-LSTM model presents a good performance on the able-bodied subjects. Compared with the BP model for angle estimation by using raw sEMG signals, this method improved some aspects of angle estimation. Such as the estimation accuracy, real-time characteristic. Based on these results, the active training by using sEMG signals can be implemented in a better manner on the upper limb rehabilitation robot for SCI patients or stroke patients. So as to help them restore the strength and function of their upper limbs.

## IV. CONCLUSION AND DISCUSSION

The main problems for the estimation of the joint angle are sEMG signals acquisition and signal processing. Raw sEMG signal without preprocessing has a poor estimation effect. The main muscles involved in the movement should play a major role in the estimation of the joint angle. The number of sEMG channels is not the more the better. Much more useless information may cause the network oscillation. Therefore, it is necessary to calculate the synergistic muscle groups related to movement. When extracting the sEMG signal features, there will also be many redundant features with high correlation. These redundant features will not only reduce the speed of model calculation, but also may affect the accuracy of estimation.

In this paper, we proposed the PSO-LSTM algorithm, and it combines the adaptive selection of optimal parameters and the LSTM regression algorithm. To continuous estimate elbow and wrist joint angles of upper limb movements based on sEMG, and analyze each joint action corresponds to synergistic muscles. It will calculate correlations between sEMG signal features and remove some highly correlated features. It not only improves the estimation accuracy but also reduces the dimensionality of the input, reducing the calculation time and improving the real-time characteristics. The study proposed in this paper improved some aspects, including the estimation accuracy and real-time characteristic. There are few points that can be improved in the future, such as the estimation accuracy of the wrist joint in continuous motion is always lower than that of the elbow joint. In order to improve the accuracy of the estimation, it is necessary to further analyze the multiple-muscle synergies of individual movement and continuous movement in future work.

## REFERENCES

[1] P. J. Treffner and M. T. Turvey, "Symmetry, broken symmetry, and handedness in bimanual coordination dynamics," *Exp. Brain Res.*, vol. 107, no. 3, pp. 463–478, Jan. 1996.

[2] J. S. Knutson, M. Y. Harley, T. Z. Hisel, S. D. Hogan, M. M. Maloney, and J. Chae, "Contralaterally controlled functional electrical stimulation for upper extremity hemiplegia: An early-phase randomized clinical trial in subacute stroke patients," *Neurorehabilitation Neural Repair*, vol. 26, no. 3, p. 239, 2012.

[3] J. Liu, Y. Ren, D. Xu, S. H. Kang, and L.-Q. Zhang, "EMG-based real-time linear-nonlinear cascade regression decoding of shoulder, elbow, and wrist movements in able-bodied persons and stroke survivors," *IEEE Trans. Biomed. Eng.*, vol. 67, no. 5, pp. 1272–1281, May 2020.

[4] D. Farina, N. Jiang, H. Rehbaum, A. Holobar, B. Graimann, H. Dietl, and O. C. Aszmann, "The extraction of neural information from the surface EMG for the control of upper-limb prostheses: Emerging avenues and challenges," *IEEE Trans. Neural Syst. Rehabil. Eng.*, vol. 22, no. 4, pp. 797–809, Jul. 2014.

[5] D. Leonardis, C. Chisari, M. Bergamasco, A. Frisoli, M. Barsotti, C. Loconsole, M. Solazzi, M. Troncossi, C. Mazzotti, V. P. Castelli, C. Procopio, and G. Lamola, "An EMG-controlled robotic hand exoskeleton for bilateral rehabilitation," *IEEE Trans. Haptics*, vol. 8, no. 2, pp. 140–151, Apr. 2015.

[6] L. Zhang, G. Liu, B. Han, Z. Wang, and T. Zhang, "SEMG based human motion intention recognition," *J. Robot.*, vol. 2019, pp. 1–12, Aug. 2019.

[7] J. L. Pons, *Wearable Robots: Biomechatronic Exoskeletons*. Hoboken, NJ, USA: Wiley, 2008.

[8] P. Artemiadis, "EMG-based robot control interfaces: Past, present and future," *Adv. Robot. Autom.*, vol. 1, no. 2, pp. 1–3, 2012.

[9] L. Vodovnik, C. Long, J. B. Reswick, A. Lippay, and D. Starbuck, "Myo-electric control of paralyzed muscles," *IEEE Trans. Biomed. Eng.*, vol. BME-12, nos. 3–4, pp. 169–172, Jul. 1965.

[10] G. Hefftner, W. Zucchini, and G. G. Jaros, "The electromyogram (EMG) as a control signal for functional neuromuscular stimulation. I. Autoregressive modeling as a means of EMG signature discrimination," *IEEE Trans. Biomed. Eng.*, vol. 35, no. 4, pp. 230–237, Apr. 1988.

[11] Y. Zeng, J. Yang, C. Peng, and Y. Yin, "Evolving Gaussian process autoregression based learning of human motion intent using improved energy kernel method of EMG," *IEEE Trans. Biomed. Eng.*, vol. 66, no. 9, pp. 2556–2565, Sep. 2019.

[12] M. Ison and P. Artemiadis, "The role of muscle synergies in myoelectric control: Trends and challenges for simultaneous multifunction control," *J. Neural Eng.*, vol. 11, no. 5, Oct. 2014, Art. no. 051001.

[13] D. Qi-Chuan, X. An-Bin, Z. Xin-Gang, and H. Jian-Da, "A review on researches and applications of sEMG-based motion intent recognition methods," *Acta Automatica Sinica*, vol. 42, no. 1, pp. 13–25, 2016.

[14] A. J. Young, L. H. Smith, E. J. Rouse, and L. J. Hargrove, "Classification of simultaneous movements using surface EMG pattern recognition," *IEEE Trans. Biomed. Eng.*, vol. 60, no. 5, pp. 1250–1258, May 2013.

[15] J. Han, Q. Ding, A. Xiong, and X. Zhao, "A state-space EMG model for the estimation of continuous joint movements," *IEEE Trans. Ind. Electron.*, vol. 62, no. 7, pp. 4267–4275, Jul. 2015.

[16] Q. Zhang, R. Liu, W. Chen, and C. Xiong, "Simultaneous and continuous estimation of shoulder and elbow kinematics from surface EMG signals," *Frontiers Neurosci.*, vol. 11, p. 280, May 2017.

[17] K. M. Steele, M. C. Tresch, and E. J. Perreault, "The number and choice of muscles impact the results of muscle synergy analyses," *Frontiers Comput. Neurosci.*, vol. 7, p. 105, 2013.

[18] M. Berniker, A. Jarc, E. Bizzi, and M. C. Tresch, "Simplified and effective motor control based on muscle synergies to exploit musculoskeletal dynamics," *Proc. Nat. Acad. Sci. USA*, vol. 106, no. 18, pp. 7601–7606, May 2009.

[19] G. Kamen and D. Gabriel, *Essentials of Electromyography*. New York, NY, USA: McGraw-Hill, 2010.

[20] B. Hudgins, P. Parker, and R. N. Scott, "A new strategy for multifunction myoelectric control," *IEEE Trans. Biomed. Eng.*, vol. 40, no. 1, pp. 82–94, 1st Quart., 1993.

[21] J. Rafiee, M. A. Rafiee, F. Yavari, and M. P. Schoen, "Feature extraction of forearm EMG signals for prosthetics," *Expert Syst. Appl.*, vol. 38, no. 4, pp. 4058–4067, Apr. 2011.

[22] L. Pan, D. Zhang, J. Liu, X. Sheng, and X. Zhu, "Continuous estimation of finger joint angles under different static wrist motions from surface EMG signals," *Biomed. Signal Process. Control*, vol. 14, pp. 265–271, Nov. 2014.

[23] M. C. Tresch, V. C. K. Cheung, and A. d'Avella, "Matrix factorization algorithms for the identification of muscle synergies: Evaluation on simulated and experimental data sets," *J. Neurophysiol.*, vol. 95, no. 4, pp. 2199–2212, Apr. 2006.

[24] A. Phinyomark, P. Phukpattaranont, and C. Limsakul, "Feature reduction and selection for EMG signal classification," *Expert Syst. Appl.*, vol. 39, no. 8, pp. 7420–7431, Jun. 2012.

[25] S. Muceli and D. Farina, "Simultaneous and proportional estimation of hand kinematics from EMG during mirrored movements at multiple degrees-of-freedom," *IEEE Trans. Neural Syst. Rehabil. Eng.*, vol. 20, no. 3, pp. 371–378, May 2012.

[26] F. Zhang, P. Li, Z.-G. Hou, Z. Lu, Y. Chen, Q. Li, and M. Tan, "SEMG-based continuous estimation of joint angles of human legs by using BP neural network," *Neurocomputing*, vol. 78, no. 1, pp. 139–148, Feb. 2012.

[27] J. Wang, Q. Hao, X. Xi, J. Cao, A. Xue, and H. Wang, "Estimation of continuous joint angles of upper limb based on sEMG by using GA-Elman neural network," *Math. Problems Eng.*, vol. 2020, pp. 1–11, Jul. 2020.

[28] C. Ma, C. Lin, O. W. Samuel, L. Xu, and G. Li, "Continuous estimation of upper limb joint angle from sEMG signals based on SCA-LSTM deep learning approach," *Biomed. Signal Process. Control*, vol. 61, Aug. 2020, Art. no. 102024.

[29] J. Chen, X. Zhang, Y. Cheng, and N. Xi, "Surface EMG based continuous estimation of human lower limb joint angles by using deep belief networks," *Biomed. Signal Process. Control*, vol. 40, pp. 335–342, Feb. 2018.

[30] Y. Hua, Z. Zhao, R. Li, X. Chen, Z. Liu, and H. Zhang, "Deep learning with long short-term memory for time series prediction," *IEEE Commun. Mag.*, vol. 57, no. 6, pp. 114–119, Jun. 2019.

[31] Y. Bowen and Q. Weiyi, "Summary on improved inertia weight strategies for particle swarm optimization algorithm," *J. Bohai Univ. (Natural Sci. Ed.)*, vol. 40, no. 3, pp. 274–288, 2019.


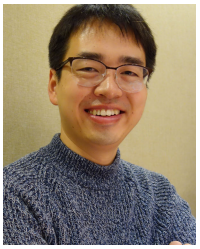

**GANG TANG** received the M.S. degree in mechanical engineering from the Harbin Institute of Technology, and the Ph.D. degree in mechanical engineering from Shanghai Jiao Tong University. His research interest includes biomechanics.

**JINQIN SHENG** received the B.S. degree in communications engineering from Hubei Normal University, Huibei, Anhui, in 2019. She is currently pursuing the M.S. degree in mechanical engineering with Shanghai Maritime University, Shanghai, China. Her research interest includes biomechanics.

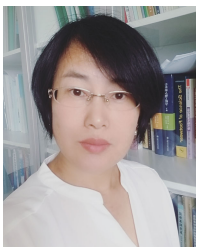

**DONGMEI WANG** received the Ph.D. degree mechanical engineering from the School of Mechanical and Power Energy Engineering, Shanghai Jiao Tong University. Her research interests include musculoskeletal system biomechanics, prosthesis design and biomechanical analysis, biomechanics in orthopedics and rehabilitation, and stress-bone remodeling simulation.

**SHAOYANG MEN** received the M.S. degree in communication and information system from the South China University of Technology, in 2014, and the Ph.D. degree in signal and information processing from the University of Nantes, in 2016. His research interests include medical image processing, signal processing, and text information extraction.